Received: 19 September 2022 | Revised: 30 June 2023 | Accepted: 28 July 2023

DOI: 10.1002/we.2860

SPECIAL ISSUE PAPER

WILEY

Advanced wind turbine control development using field test analysis for generator overspeed mitigation

Mandar Phadnis[1] | Daniel Zalkind[2] | Lucy Pao[3,4]

[1]Aerospace Engineering Sciences, University of Colorado Boulder, Boulder, Colorado, USA

[2]National Renewable Energy Laboratory, Golden, Colorado, USA

[3]Electrical, Computer and Energy Engineering, University of Colorado Boulder, Boulder, Colorado, USA

[4]Renewable and Sustainable Energy Institute, Boulder, Colorado, USA

Correspondence
Mandar Phadnis, Aerospace Engineering Sciences, University of Colorado Boulder, Boulder, CO, USA.
Email: mandar.phadnis@colorado.edu

Funding information
Advanced Research Projects Agency—Energy (ARPA-e) ATLANTIS Program, Grant/Award Number: DE-AR0000667; Palmer Endowed Chair Professorship at the University of Colorado Boulder; Hanse-Wissenschaftskolleg; National Renewable Energy Laboratory, Grant/Award Number: DE-AC36-08GO28308

Abstract

Turbulent and gusty wind conditions can cause generator overspeed peaks to exceed a threshold that then lead to wind turbine shutdowns, which then decrease the energy production of the wind turbines. We derive so-called "gust measures" that predict when generator overspeed peaks may occur. These gust measures are then used to develop advanced controllers to mitigate generator overspeed peaks so that wind turbines can operate more robustly in difficult wind conditions without exceeding generator overspeed thresholds that would lead to turbine shutdown events. The advanced controllers are demonstrated in nonlinear aeroelastic simulations using the open-source wind turbine simulation tool OpenFAST. To increase the realism of the simulations, they are run using field-replicated wind conditions and a wind turbine model based on data from an experimental field campaign on a downscaled demonstrator of a novel extreme-scale, two-bladed, downwind rotor design.

KEYWORDS
advanced control, downwind, field test, gust estimation

1 | INTRODUCTION

In recent years, wind energy has seen rapid growth in adoption across the world. There has been a concerted effort in the wind power industry to bring down the levelized cost of energy (LCOE) of wind turbines in order to compete with fossil and other renewable energy sources.[1] The power generated by a single wind turbine is proportional to its rotor swept area and to the cube of the wind speed.[2] The wind speeds usually increase with altitude. Both of these factors have resulted in wind turbines becoming larger in terms of rotor radius and taller in terms of tower height.[3] Modern multi-megawatt wind turbines face complex control challenges. For example, turbulent wind can result in poorly regulated generator speed and power fluctuation. Particular gust patterns in wind have been observed to cause overspeed peaks in the generator speed response.[4–6] Generator overspeeding can be detrimental if it exceeds the turbine's overspeed shutdown threshold which can increase downtime and reduce the annualized energy production (AEP). In this research, we develop a gust-measure-based advanced control technique to improve generator speed regulation in highly turbulent and gusty winds. Gust-measure-based control has been previously shown to improve generator speed regulation under problematic wind gusts.[4,5] We develop a variation of the gust measure to further improve generator speed regulation under wind gusts near the rated operation of the wind turbine. This advanced control is tested in simulation, using data from a field experiment of a novel two-bladed downwind turbine, under simulated realistic wind conditions experienced by an experimental turbine at the test site.

The overwhelming proportion of wind turbines currently in operation are three-bladed upwind turbines, having a symmetrical configuration of three blades, 120° apart, with the rotor facing the wind and the nacelle and tower in its wake. In this configuration, the aerodynamic thrust on the rotor causes the blades to deflect toward the tower. A tower strike by the blades is typically avoided by increasing the rotor coning and/or shaft tilt angles and by designing the blades to have enough stiffness and mass to maintain a sufficient tower clearance under all design load cases (DLCs). As rotors become larger in size, the stiffness constraint on these longer upwind blades continues to add mass and cost to the rotor while also pushing the boundaries of blade fabrication. The Segmented Ultralight Morphing Rotor (SUMR)[7] is a project funded by the U.S. Department of Energy[8,9] to develop a novel, extreme-scale, two-bladed, downwind turbine design, specifically exploring the advantages of using lightweight, ultra-flexible blades in a two-bladed, downwind configuration as opposed to the conventional three-bladed, upwind setup, with regard to reducing the blade stiffness and rotor mass in order to lower the LCOE. In downwind rotors, the blades deflect away from the tower under aerodynamic thrust, thus relaxing the constraint on blade stiffness, allowing for lighter, flexible blades that can align with the dynamic loads in the direction of the wind. The SUMR team members have designed a 50 MW two-bladed downwind concept rotor called SUMR-50.[10,11] Earlier iterations of 13.2 MW turbine (SUMR-13) designs showed potential for reduced rotor mass, capital costs, and LCOE.[12] To validate these design results, an experimental test campaign was undertaken to manufacture a scaled SUMR-13-based demonstrator rotor for field testing. Since construction costs of a 13.2 MW turbine would be exorbitant, an aero-gravo-elastically downscaled model was designed.[13,14] The downscaled 53.38 kW turbine called SUMR-Demonstrator (SUMR-D) was manufactured, deployed, and tested extensively on the National Renewable Energy Laboratory's (NREL's) two-bladed Controls Advanced Research Turbine (CART2) platform.[15]

The data from these field tests[16] provide an opportunity to assess the performance of the baseline (BL) turbine controller. We primarily study the power curve, the flapwise blade loads, the generator speed, and actuator responses. We observe that particular gust patterns in near- and above-rated wind conditions resulted in overspeed peaks in generator speed response. Improvements to the field-tested BL control are made using gust measure(s) to mitigate generator overspeed events in the presence of such particular wind gusts. Due to the unavailability of the field experiment setup for further testing of the gust-measure-based advanced controller, wind measurements from the field sensors are used to replicate the turbulent wind conditions from the test site in simulation. Generator speed and actuator responses from the field-replicated simulations are compared against field data to reasonably match the model to the test turbine. The advanced control is then tested on this verified model in simulation with a high confidence that the effectiveness of the advanced controllers would have transferred to the actual turbine had further field testing been possible.

Various advanced control techniques are being developed in the literature to address the challenges arising due to longer blades and taller towers of modern scale wind turbines. These control techniques (among other objectives) aim to improve generator speed regulation, reduce structural loads, and increase the AEP. Individual pitch control (IPC)[17] is widely used in industry and academia to address the periodic once-per-revolution fatigue loading on the turbine blades at the cost of increased blade pitch travel. In contrast to collective pitch control, IPC pitches each blade individually to counter the effects of asymmetric loading across the rotor plane caused by turbulence and wind shear. IPC can be implemented using methods such as multi-blade coordinate transformation (MBC)-based proportional–integral (PI) control or state-feedback-based linear quadratic regulator (LQR) control.[18,19] Alternatively, peak shaving (PS) is a control technique used to limit high loads at near-rated operation.[5,20] Wind turbines experience peak mechanical loading near their rated operating wind speed due to the maximal aerodynamic thrust on the rotor. These loads primarily affect the blade flapwise and tower fore–aft moments. PS uses generator speed feedback or a wind speed estimate to monitor the proximity of a turbine to its rated operation and de-rates the turbine when it approaches this high load state by pitching the turbine blades while transitioning from below-rated to above-rated operation. This limits the peak of the load curve, albeit also causing a reduction in power capture and AEP. Recently, distributed aerodynamic control using actuated trailing edge flaps (TEFs) has also been studied to reduce power fluctuations and blade root loads in large wind turbines such as the Big Adaptive Rotor.[21–23] TEFs provide a high-bandwidth localized control mechanism with added cost and manufacturing complexity. De-rating at high wind speeds for extreme-scale wind turbines has also been studied to reduce loading on the turbine blades while minimizing the decrease in AEP.[5] The control techniques in this research dynamically de-rate the wind turbine based on potentially difficult incoming gusts by employing gust measures derived from recent wind speeds. The gust measure has been shown to improve generator speed regulation for the three-bladed upwind NREL-5MW reference turbine[5] and the novel two-bladed downwind SUMR-13 turbine.[4] In this research, a proposed variation of the gust measure is developed, improving its performance in reducing generator overspeed peaks in the near-rated region. The gust measure and the proposed modified gust measure are shown to reduce generator overspeed occurrences compared to the BL controller in high-turbulence intensities using field test data of the SUMR-D turbine replicated within simulation.

The remainder of this paper is organized as follows. Section 2 details the SUMR-D wind turbine along with the BL controller used for testing. Section 3 summarizes the field test experiment, and the field measurements are analyzed for wind resource assessment. In Section 4, the simulated model of the SUMR-D turbine is compared against the field test data, for the operational design load case 1.2 (DLC 1.2) and for simulations under environmental conditions from the field test. This section also explains the process of using wind measurements from the field test to replicate field wind conditions in simulation. Section 5 extends a gust measure and implements advanced control techniques using the (modified) gust measure(s) to mitigate generator overspeed events. Section 6 concludes this work and discusses future directions.

2 | SUMR-D

The SUMR-13 design was the result of a multi-institutional, iterative aerodynamic, structural, and control development process. The resultant turbine design had a rotor radius of 107 m, with a rated wind speed of 11.3 m/s. The SUMR-D test rotor is a one-fifth scaled version of the SUMR-13 (13.2 MW) design, downscaled using a gravo-aeroelastic scaling (GAS) method to match the nondimensional geometry, flapwise blade deflections, and dynamics of SUMR-13.[13–15]

The SUMR-D was installed and tested on the CART2[24] at NREL's National Wind Technology Center (NWTC) in Colorado, USA. The CART2 is typically a 43.3 m diameter, two-bladed, upwind rotor with 600 kW rated power at 162 kNm rated torque. It also has a 0° coning and a 3.77° shaft tilt. To meet the downwind, highly coned (12.5° at operation) requirements for the SUMR-D experiments, various modifications had to be made to the CART2, including de-rating the turbine from 600 to 53.38 kW, installing coning adapters outboard of the pitching motors for each blade, offsetting the yaw control to have the rotor face downwind during operation, and so on.[15] Conversely, since SUMR-D was tested with an existing turbine, not all components, including the tower and the hub, were available for downscaling to the exact proportions.[14] The relevant parameters of the final test configuration of the SUMR-D on the CART2 are listed in Table 1. Each of the turbine parameters was either driven by the SUMR-D blades design or CART2 platform constraints.

2.1 | Wind turbine

The SUMR-13 was designed iteratively, between multiple institutions, with the aerodynamic designs developed by the University of Virginia and the University of Illinois, the structural designs by the University of Texas at Dallas, and the controls development by the University of Colorado Boulder and the Colorado School of Mines.

The aerodynamic design was developed using the inverse design tools PROPID[25] and PROFOIL.[26] PROPID develops the rotor geometry to meet rated power, optimal tip-speed ratio, rated wind speed, and axial induction as prescribed. PROFOIL provides airfoil shapes for desired

TABLE 1 SUMR-D + CART2 wind turbine parameters.[15]

Parameter	SUMR-D rotor	CART2 turbine
Blade length	20.87 m	-
Coning adapter length (see Figure 5)	-	0.50 m
Hub radius	-	1.38 m
Fine pitch angle	−5°	-
Blade mass	985.6 kg	-
Tower height	-	34.86 m
Shaft tilt	-	3.77°
Rotor coning	12.50°	-
Rated power	53.38 kW	-
Rated wind speed	5.75 m/s	-
Cut-in wind speed	3 m/s	-
Cut-out wind speed	11 m/s	-
Rated rotor speed	21.47 RPM	-
Rated generator speed	926.75 RPM	-
Rated generator torque	550 Nm	-
Gearbox ratio	-	43.17
Tip-speed ratio	9.50	-
Overhang	-	3.86 m
Hub mass	-	5852 kg
Hub inertia	-	15,000 kg·m^2
Generator inertia	-	34.40 kg·m^2
Generator overspeed shutdown threshold	1100 RPM	-

Note: Since the SUMR-D turbine is a combination of the SUMR-D rotor on the CART2 platform, the column location of each parameter indicates whether it is derived from the SUMR-D scaled rotor or the CART2.

velocity profiles.[15] The aerodynamic design process is explained in detail in Ananda et al.[27] The designed SUMR-13 blades were geometrically downscaled for a final SUMR-D blade length of 20.87 m. Since the CART2 had no rotor coning angle, a coning adapter had to be designed, manufactured, and installed outboard of the pitch actuators at the hub to achieve the SUMR-D coning angle of 12.5°. With a coning adapter of 0.5 m length and the CART2 hub radius of 1.38 m, the SUMR-D radius projected onto the rotor plane equaled 22.26 m. The structural design for SUMR-D was conducted using ANSYS APDL[28] to meet the scaling parameters and safety requirements at the NWTC site and was verified for loads against nonlinear aeroelastic simulations in OpenFAST.[15,29]

2.2 | BL controller

The SUMR-D BL control inherited its base structure from the SUMR-13 controller detailed in Zalkind et al.[7] However, due to non-ideal aerodynamic scaling and to match the nondimensional frequencies and tip deflections to SUMR-13, the controller was retuned and modified significantly across multiple iterations.[15] This section provides the structure and parameters of the final BL controller that was used in the field test.

The SUMR-D BL control has two main operating regions, as shown in Figure 1: Region 2 (R2) operation is active in below-rated conditions, where generator torque is actuated to maximize power output at a given wind speed, and Region 3 (R3) operation is active in above-rated conditions, where the turbine blades are collectively pitch-actuated to manipulate the aerodynamic torque on the rotor to regulate the power output to the rated capacity of the turbine. Region 1 (R1) and Region 4 (R4) are nonoperating regions where the wind conditions are either below the cut-in or above the cut-out wind speed, and the turbine is shut down. In order to reduce power and loads fluctuations during the switching of the control regions, there are linear transition regions, Region 1.5 (R1.5) and Region 2.5 (R2.5), as shown in Figure 2.

2.2.1 | Generator torque control

The usual objective of the generator torque control is to maximize the wind turbine power capture at wind speeds below the rated wind speed of the turbine. Thus, generator torque control is primarily active in below-rated regions (R1.5, R2, and R2.5). For SUMR-D, the torque control implemented a lookup-table-driven control law scheme based on the generator speed feedback signal.[7] In R2, which forms the majority of below-rated operation, the nonlinear optimal control law is given as[2]

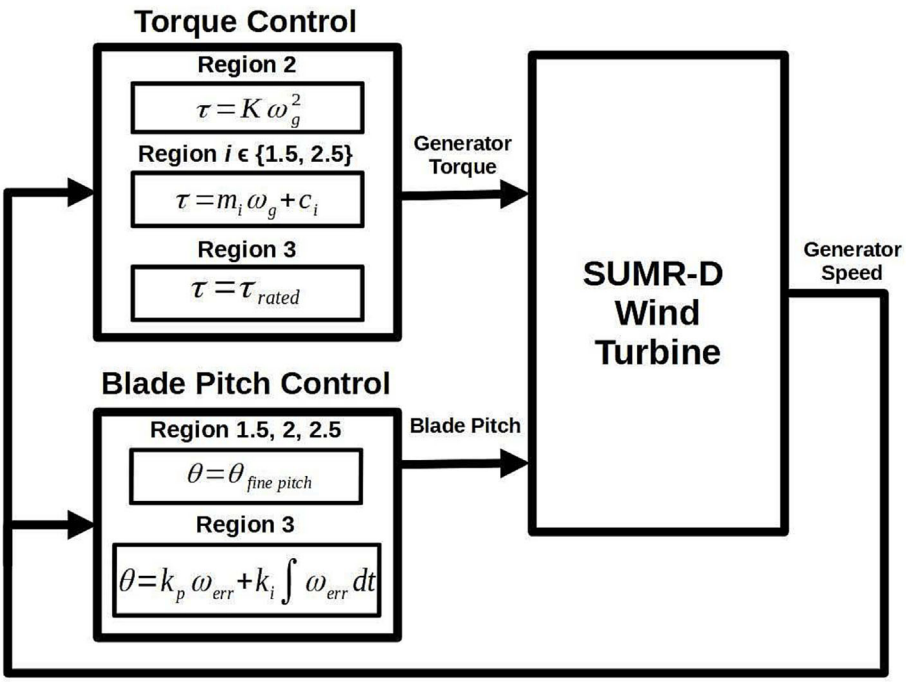

FIGURE 1 SUMR-D baseline controller structure. ω_{err} is the difference between the generator speed and the rated generator speed, θ is the current blade pitch angle, and $\theta_{finepitch}$ is the optimal blade pitch angle that maximizes the aerodynamic torque on the rotor.

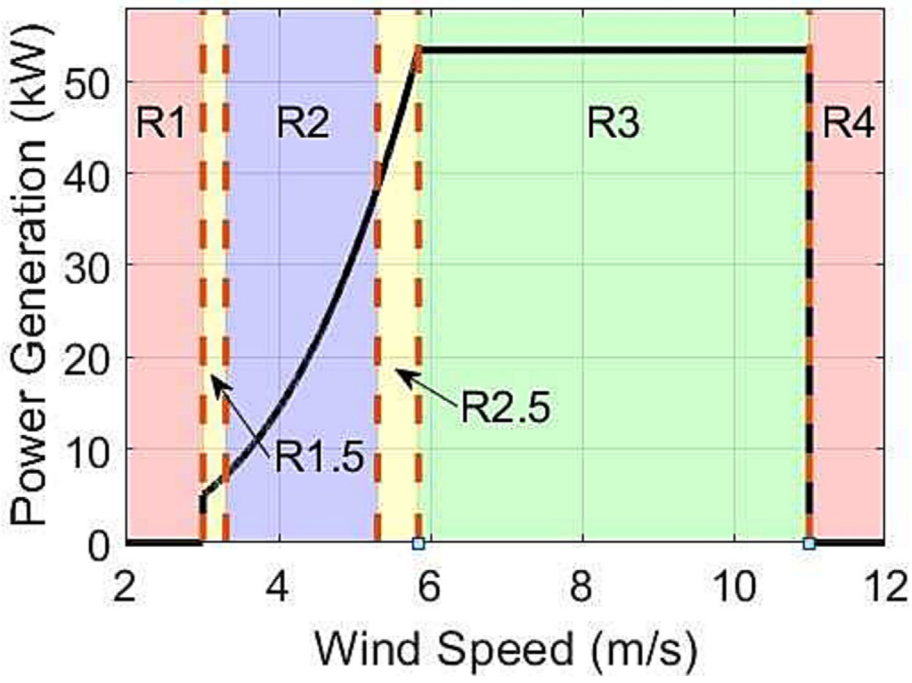

FIGURE 2 SUMR-D ideal power curve with control regions R1–R4.

$$\tau_g = k_{opt}\omega_g^2, \tag{1}$$

where τ_g is the generator torque, k_{opt} is the optimal gain, and ω_g is the generator speed. Equation (1) is used to keep the wind turbine operating near its maximum power coefficient $C_{p,max}$. The optimal constant k_{opt} is given as[2]

$$k_{opt} = \frac{\pi\rho R^5 C_{p,max}(\cos\beta_c)^2}{\lambda_{opt}^3 G^3}, \tag{2}$$

where ρ is the air density, R is the rotor radius, $C_{p,max}$ is the maximum power coefficient, β_c is the rotor coning angle, λ_{opt} is the optimal tip-speed ratio corresponding to $C_{p,max}$, and G is the gearbox ratio. The cosine factor is included to account for the effects of the coning angle on rotor aerodynamic torque. The transition regions R1.5 and R2.5 are governed by linear control laws of the form:

$$\tau_g = m_i\omega_g + c_i, \tag{3}$$

where m_i and c_i are the slope and intercept for region $i \in \{1.5,2.5\}$, respectively. The lookup table for torque control along with the tuning parameters are summarized in Table 2.

2.2.2 | Collective blade pitch control

The primary objective of blade pitch control is to regulate the generator speed and power to the rated capacity of the wind turbine. SUMR-D employs a collective blade pitch scheme using gain-scheduled PI control[7]:

$$\begin{aligned} \theta &= k_P(\theta)\omega_{err} + k_I(\theta)\int\omega_{err}dt, \\ \omega_{err} &= \omega_g - \omega_{ref}, \end{aligned} \tag{4}$$

where θ is the collective blade pitch command, $k_P(\theta)$ and $k_I(\theta)$ are pitch-scheduled proportional and integral gains, ω_g is the generator speed, and ω_{ref} is the reference generator speed setpoint. Since the aerodynamic torque on the rotor is nonlinearly related to the blade pitch angle, the k_P

TABLE 2 SUMR-D torque control lookup-table parameters.

Control region	Start (>RPM)	End (<RPM)	Control law	Parameters
Region 1	0	258.98	$\tau_g = 0$	NA
Region 1.5	258.98	310.78	$\tau_g = m_{1.5}\omega_g + c_{1.5}$	$m_{1.5} = 8.901$ Nms/rad, $c_{1.5} = -243$ Nm
Region 2	310.78	834.08	$\tau_g = k_{opt}\omega_g^2$	$k_{opt} = 0.0459$ Nms^2/rad^2
Region 2.5[a]	834.08	880.415	$\tau_g = m_{2.5}\omega_g + c_{2.5}$	$m_{2.5} = 41.2052$ Nms/rad, $c_{2.5} = -3248.9$ Nm
Region 3	880.415	NA	$\tau_g = \tau_{rated}$	$\tau_{rated} = 550$ Nm

[a]Region 2.5 begins at 90% and ends at 95% of the rated generator RPM.

TABLE 3 SUMR-D blade pitch control parameters.

Parameter	Description	Value
$k_P(0)$	Proportional gain at $\theta = 0$	0.0812 s
$k_I(0)$	Integral gain at $\theta = 0$	0.0143
θ_k	Blade pitch angle at which $(\delta P/\delta\theta)$ sensitivity doubles	6.35°

TABLE 4 SUMR-D field sensors.

Sensor	Height
Nacelle cup anemometer	36.6 m
Nacelle wind vane	36.6 m
Met mast cup anemometer 1	3 m
Met mast wind vane 1	3 m
Met mast cup anemometer 2	15 m
Met mast wind vane 2	15 m
Met mast cup anemometer 3	36 m
Met mast wind vane 3	36 m
Met mast cup anemometer 4	58.2 m
Met mast wind vane 4	58.2 m
Met mast 3D sonic anemometer	36.6 m

and k_I gains are scheduled based on the sensitivity of generator power to the blade pitch angle $(\delta P/\delta\theta)$. The gain scheduling factor for the SUMR-D blade pitch control is given by $(1+\theta/\theta_k)$ where θ_k is the angle at which the sensitivity doubles, as detailed in Zalkind et al.[5] The blade pitch control design parameters used for the SUMR-D turbine are listed in Table 3.

3 | SUMR-D EXPERIMENT

The SUMR-D experiment was conducted from October 2019 to March 2020 at NREL's NWTC facility near Boulder, Colorado. The test setup mainly consisted of the SUMR-D blades and coning adapter installed on the CART2, with the primary meteorological (met) mast located 88 m upstream in the dominant wind direction. The met mast has four cup anemometers and four wind vanes at different heights and a three-dimensional (3D) sonic anemometer at hub height. The CART2 nacelle has a cup anemometer and wind vane at hub height. The wind sensors are summarized in Table 4. The operational test matrix required a minimum of six 10 min data sets collected for each 1 m/s wide wind speed bin, from 4 to 10 m/s. The operational test matrix was completed beyond its requirements, as shown in Table 5. Of the recorded operational data, only the data sets where the operational controller was active all of the time are included in this analysis. The SUMR-D test setup was subsequently taken out of operation and dismantled in early 2022.

The field test data provide a wealth of information to assess the performance of the SUMR-D turbine under real-world conditions. In order to conduct a fair performance assessment, it is first important to understand the wind resource to select valid data sets and perform necessary adjustments to the data before analysis. The NWTC site is known for high-turbulence wind conditions. Site conditions like turbulence, shear, and

TABLE 5 SUMR-D operational test matrix.

Wind bin	Required 10-min data sets	Recorded 10-min data sets
4–5 m/s	6	53
5–6 m/s	6	43
6–7 m/s	6	39
7–8 m/s	6	41
8–9 m/s	6	26
9–10 m/s	6	15
Totals	36	217

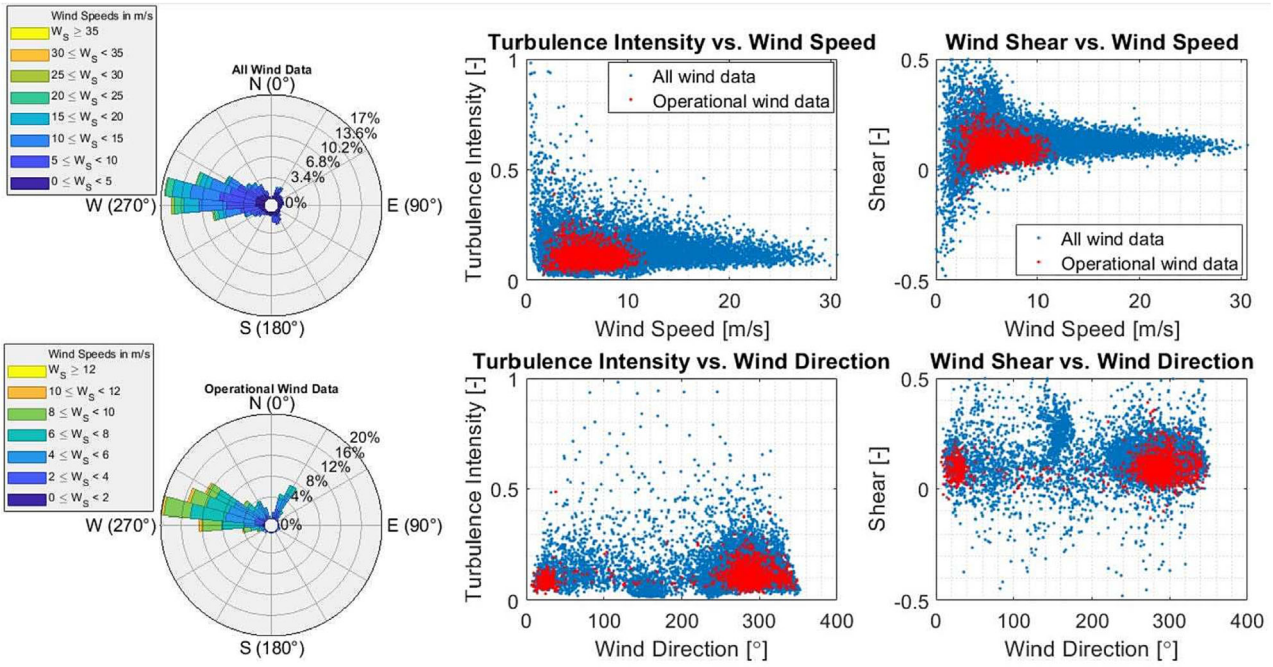

FIGURE 3 NWTC site conditions during SUMR-D experiment window. Each data point represents a 1 min average of the time series recorded at 400 Hz.

air density can have a significant impact on the power performance of a wind turbine.[30,31] As such, there is value in accounting for site conditions before any power performance analysis is conducted.

Figure 3 shows the wind roses[32] for wind during the experiment and for operational cases. It is clear that the dominant wind direction is from the west. Turbulence intensity is calculated as the ratio of the standard deviation to the mean wind speed at hub height. Wind shear is calculated through a power-law fit across the wind speed measurements at various heights on the met mast.[31] Figure 3 shows 1 min time-averaged data points for turbulence intensity at hub height and wind shear as a function of wind speed and wind direction. Since a limited amount of operational data is available, averaging is performed over 1 min bins to have a higher resolution across the operational field test data. The average turbulence intensity measured during the field test was 18% with a mean wind speed of 9 m/s, and the turbulence intensity near the rated wind conditions of the SUMR-D was 18.78%. The turbulence intensity under operational wind speeds was mostly bounded between 5% and 25%, whereas the wind shear under operation varied from 0.0 to 0.2. These parameters were used to guide the operational DLCs used to study the model performance compared to the test turbine.

4 | MODEL COMPARISON

Due to project constraints, the SUMR-D was unavailable for field testing of further advanced controller developments beyond the BL controller testing that was completed. Since the SUMR-D has since been dismantled, control techniques developed in this research could only be tested in simulation. To build confidence that the control developments would have translated reliably to the actual test turbine, the simulation model is

verified to reasonably match the test turbine by comparing the test data against operational DLCs and field wind conditions replicated in simulation. The simulated performance of the field-tested controller is then used as a BL to evaluate the benefits of advanced control in regulating generator speed.

4.1 | Operational DLC: DLC 1.2

International Electrotechnical Commission (IEC) DLC 1.2[33] is the operational case with the normal turbulence model (NTM) as defined by IEC across wind speeds from cut-in to cut-out. We use DLC 1.2 with class 1A turbulence characteristics for wind speeds from 3 to 11 m/s at 1 m/s intervals and six random seeds at each wind speed to simulate the operational performance of SUMR-D using OpenFAST. An NTM provides a turbulence intensity that decreases with wind speed, as is observed in the measured data. Additionally, we set the wind shear to 0.14 to be close to site-measured values. Effects of wind veer and yaw misalignment between the rotor and mean wind direction have not been accounted for in this analysis. In Figure 4A, we see that under turbulence, the SUMR-D generated higher power at lower winds and lower power at higher, near/above-rated winds as compared to the steady (no turbulence) wind case. This difference, also seen with the DLC 1.2 simulated power curve, is an expected effect of turbulence on the power curve.[30] OpenFAST is found to significantly underestimate the rotor torque, especially in below-rated operation. This results in a lower simulated power capture in R2. It is noted that the mean power generated during the field test was higher than but within one standard deviation of the simulated power under DLC 1.2. Differences between the designed and manufactured blade properties may have resulted in the differences in rotor torque and hence the power curve.

Comparing the flapwise blade root loads in Figure 4B, there is an agreement in the mean blade loads between the test data and DLC 1.2 simulation up to wind speeds of 4 m/s. In the near-rated region, OpenFAST generally overestimated the flapwise blade loads until 6.5 m/s, beyond which the measured loads, on average exceed the simulated loads. We can attribute this to the aerodynamic differences in the blades due to manufacturing deviations and the unmodeled dynamic rotor coning angle introduced by the installation of a coning adapter outboard of the pitch drive.[15] The latter caused the rotor coning angle for SUMR-D to be a function of the blade pitch angle, as shown in Figure 5, effectively increasing the rotor swept area as the blade pitch increased at higher wind speeds. This dynamic enforced by manufacturing requirements is not present in the simulations, where the rotor coning angle remains constant. The flapwise load signal is also prone to sensor bias which can further affect the accuracy of the measurements.

4.2 | Replicating field test results in simulation

The SUMR-D simulation model is built using the OpenFAST aeroelastic wind turbine simulator. The aerodynamic properties of the turbine blades are defined using the AeroDyn version 15 module of OpenFAST. The structural properties of the blades and towers are described using ElastoDyn. A more precise BeamDyn module is not used for blade structural description to avoid excessive computational cost and complexity. Simulated wind is generated using the TurbSim tool to reasonably replicate the wind conditions experienced during field testing by using available

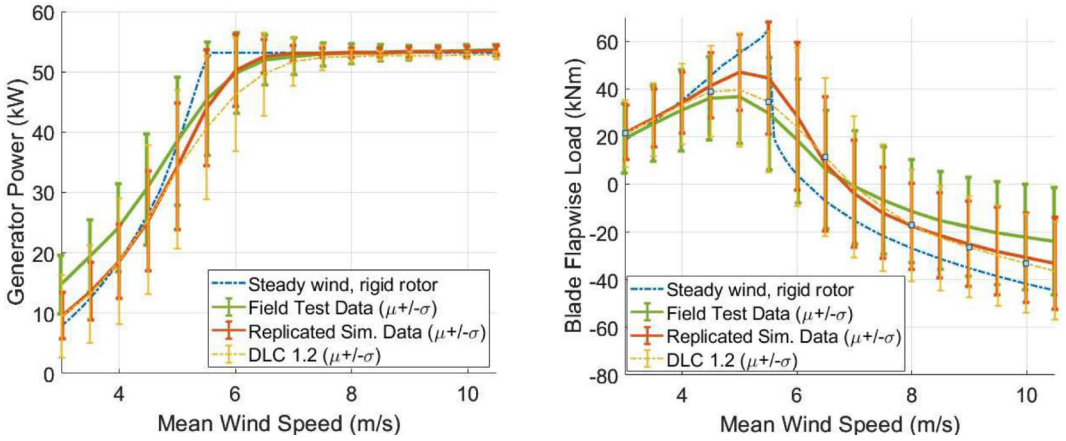

(A) SUMR-D: power curves comparison. μ and σ represent the bin average and standard deviation, respectively.

(B) SUMR-D flapwise blade loads. μ and σ represent the bin average and standard deviation, respectively.

FIGURE 4 Comparison of SUMR-D OpenFAST simulations (steady wind and DLC 1.2) and operational field test data.

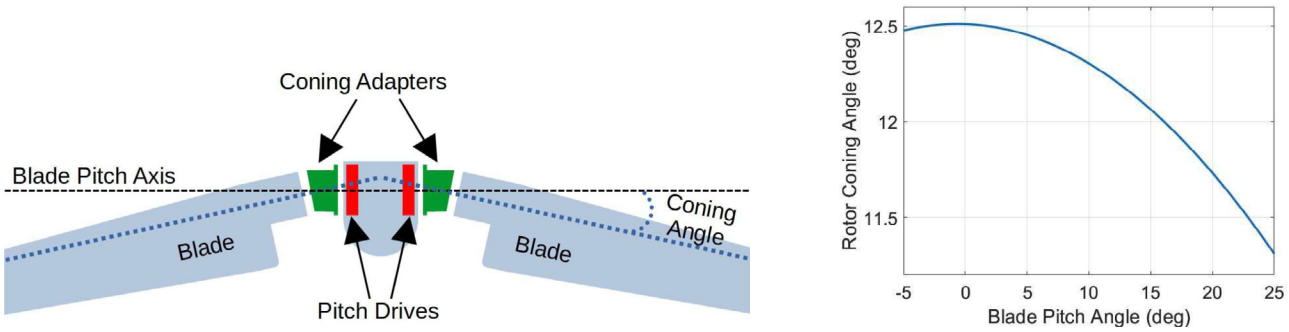

(A) Coning adapter diagram

(B) Coning angle as a function of blade pitch

FIGURE 5 SUMR-D coning adapter setup and its unmodeled effect on the rotor coning angle.

wind sensor measurements, and then applied in OpenFAST simulations using the InflowWind module. The controller is developed using Simulink[34] to match the controller tested in the field and then integrated with OpenFAST through the ServoDyn module.

To use the nonlinear aeroelastic SUMR-D simulated model for advanced control design, the operational site conditions are replicated within the simulation. This helps to verify that the simulation is a fair representation of the actual wind turbine and to build confidence that the benefits of advanced control development would carry over to the actual wind turbine when it is not possible to test the new controller in the field. The turbulent wind field across the rotor plane is a critical element in achieving a reasonable match between simulation and field test. The field wind conditions are recreated in simulation using the various wind speed sensor measurements from the field data. First, a three-dimensional (3D) wind speed input vector, $[u,v,w]^T$, with u, v, and w being the downwind, crosswind, and vertical directions, respectively, is generated as follows. The nacelle wind speed measurement is down-sampled to the simulation time step and used as the downwind direction u. Being upstream of the downwind coned rotor, it was verified that the axial induction bias of the nacelle wind speed measurements deviated only a few percent from the hub height wind speed measurements at the met mast. The sonic anemometer on the met mast provides the v and w direction measurements 88 m upwind of the turbine. These are used to obtain normal distributions that are used to randomly sample the crosswind and vertical directions, thus completing the 3D wind speed vector. The nacelle wind speed measurement is also used to calculate the input turbulence intensity and the mean wind speed for the simulation. Finally, the wind speed measurements at different heights on the met mast are used to calculate a wind shear exponent that fits a power-law curve through the mean wind speeds at each height for a given simulation. The wind speed input vector, turbulence intensity, mean wind speed, and power-law exponent are input to TurbSim version 2 (see Jonkman[35]) to generate the full field turbulent wind file. The 3D wind speed vector is input as the desired time series at hub height. TurbSim generates the time series at other grid points accounting for the vertical wind shear and the general spatial coherence model as detailed in Jonkman.[35] For each OpenFAST simulation, the first 100 s were dropped from the analysis to remove the simulation transients. Contiguous 5 min operational data sets were merged into longer data sets to minimize the transient data to be discarded. This resulted in the shortest simulation wind field to be of 5 min in duration and the longest simulation to be of 1 h in duration.

The BL controller is used with SUMR-D models and the replicated test-site wind fields to compare the simulation outputs with field test data. In Figure 4A, we see that the power curve matches well for the field-replicated wind simulations in near- and above-rated wind speeds. This is the critical region of operation where the advanced control techniques tested in this study are active. Figure 4B shows trends similar to those between the field test data and DLC 1.2. The flapwise blade load is over predicted in near-rated operation and under predicted at high wind speeds. Figure 6 shows the wind input at hub height, actuator responses, generator speed, and power output as measured in the field (in blue) for a 1 h contiguous time series. It is overlaid with simulation data (in red) obtained when using the BL controller, SUMR-D OpenFAST model, and a replicated wind field with the time series matching the hub height wind speed measurement. While there is a good match between the field test data and the simulation, not all of the wind field is known. In addition to the possible differences between the model and the test turbine due to manufacturing errors and the coning adapter, the field-replicated wind simulations also do not account for rotor yaw misalignment errors. Given these sources of discrepancies, there are some differences in the higher frequencies and sensitive conditions like in near-rated winds, where the control switches between R2 and R3. Despite these differences, the match is considered reasonable enough to pursue advanced controller development and evaluation using the simulation model of both the SUMR-D and the test-site wind conditions.

5 | ADVANCED CONTROL DEVELOPMENT

As has also been noted for the SUMR-13 and NREL-5 MW reference wind turbine,[4,5] a lull in wind followed by a rising gust is observed to cause a peak in generator speed response in the SUMR-D. A further observation is that, the severity of the peak is higher if the control switches from

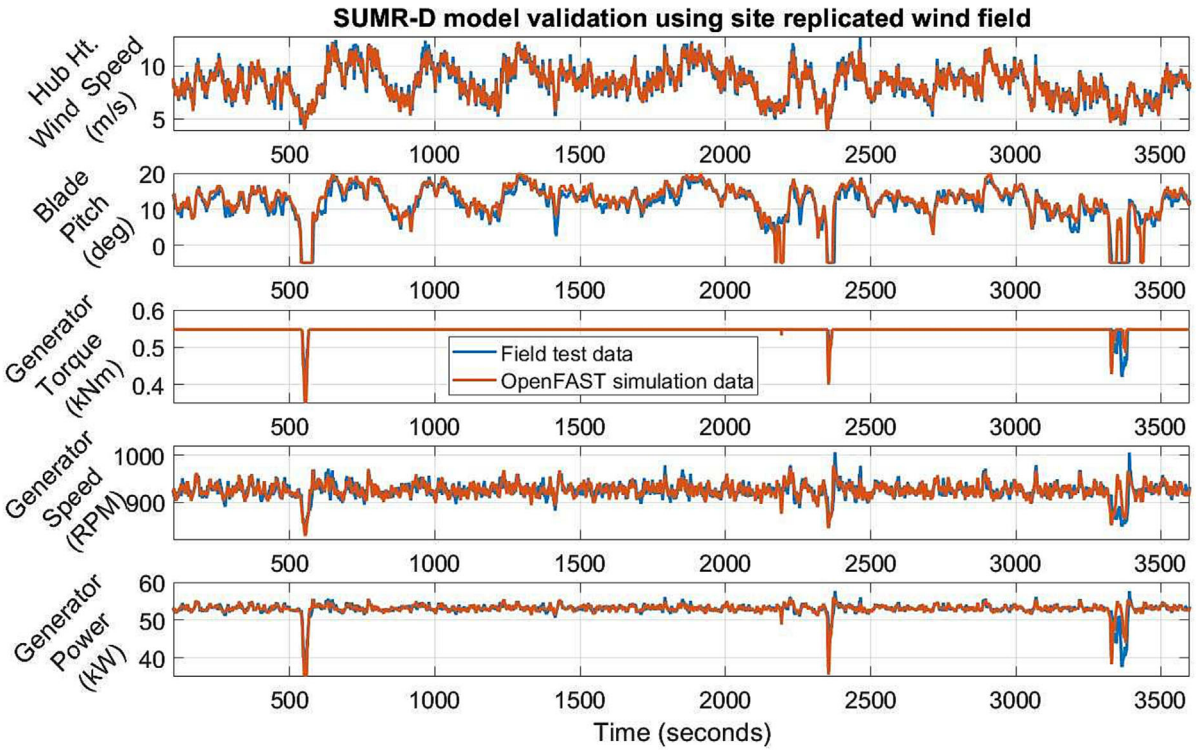

FIGURE 6 Comparison between the SUMR-D turbine and its simulation model using a 1-h-long field test data set and a field-replicated wind simulation.

R2 to R3 during the rising gust. A look at the ensemble trend in Figure 7 in the proximity of these generator speed peaks gives us insight into this behavior. To detect the peaks, the generator speed signal is filtered using a moving average over a span of 2 s to remove the high-frequency noise. The local maxima above a certain threshold in generator speed peaks are considered. The peaks in the field data are generally more severe than in simulation, due to unmodeled differences in the simulated turbine, sensing errors, and variations in the wind across the rotor plane. In Figure 7, we take the highest 30 generator speed peak occurrences for each of the following: those over 970 RPM from SUMR-D simulations (faint red) and those over 985 RPM from SUMR-D field data (faint blue), with the difference in the thresholds attributed to the mismatch between simulation and site data. The peaks are then aligned such that every peak occurs at $t_{peak} = 50$ s. We look at the preceding 50 s and following 10 s of wind speed, generator speed, blade pitch angle, and generator torque signals for each instance. An ensemble average across time for the aligned peak instances shows a trend. The wind speed on average shows a lull followed by a positive gust with a corresponding dip, rise, peak, and drop in the generator speed. The blade pitch and generator torque actuator signals show that, on average, the control is in R2 before the peak and in R3 after the peak. This is clear from the ensemble average generator torque saturating just before t_{peak}.

A "gust measure" developed in Zalkind et al[5] is used to quantify such wind gusts as a way to predict a generator speed peak occurrence. Wind conditions replicated from the field test are used in fully nonlinear aeroelastic simulations within the OpenFAST framework. Having an agreement between simulation and field cases for the BL controller provides a validation of the gust measure used in advanced control for improvements in generator speed regulation. In this study, we further propose a modified gust measure to account for the likelihood of a wind sequence causing the controller to switch modes,[6] resulting in more severe generator speed peaks. The (modified) gust measure(s) are then evaluated in simulation for their abilities to mitigate undesirable peaks in generator speed.

5.1 | Gust measure

The nacelle cup anemometer measuring wind speed at the rotor is used in the following analysis to calculate the gust measure. Being a downwind rotor, this measurement taken upstream from the highly coned downwind rotor is more reliable for SUMR-D analysis than it is for traditional upwind configurations. Implementation of a wind speed estimator for gust measure estimation is left for future work.

The gust measure from Zalkind et al[5] is briefly summarized here and implemented on the SUMR-D field data and simulations. A window of wind speeds is used:

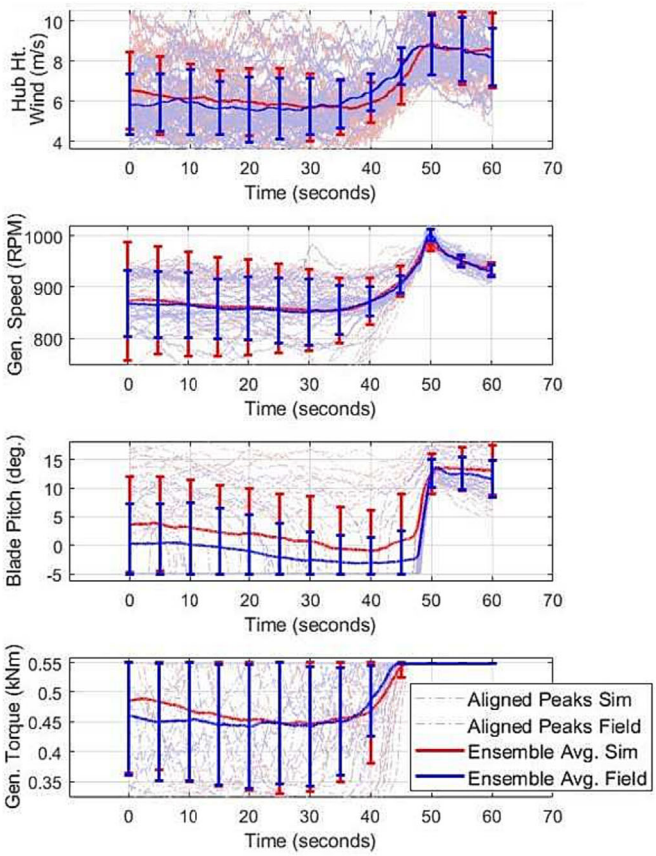

FIGURE 7 Aligned generator speed peaks. Solid lines are the ensemble averages of the wind, generator speed, blade pitch, and generator torque for 50 s prior to and 10 s after a generator speed peak event. Blue curves represent field data, and red curves represent field-replicated simulation data. Faint lines are the 30 highest individual generator speed peak events aligned at $t = 50$ s for field data and simulation. Due to differences in the simulation model and test turbine, the individual instances do not correspond to same time stamps.

$$U_{window} = \{u(t - t_r)\}_{r=0,\ldots,N}, \tag{5}$$

where $u(t_i)$ is the wind speed at time t_i and a history of N past wind speeds are used, counted using the index r. The time delays

$$t_r = r\Delta t \tag{6}$$

are spaced Δt seconds apart. A set of weighted differences between the current wind speed $u(t)$ and the delayed wind speeds is calculated:

$$\Delta U_{window} = \{w_{ur}[u(t) - u(t - t_r)]\}_{r=0,\ldots,N}, \tag{7}$$

where linear weights prioritize more recent samples:

$$w_{ur} = \frac{r}{N} + \left(1 - \frac{r}{N}\right) w_{u0}, \qquad r = 0,\ldots,N, \tag{8}$$

with $w_{u0} > 1$ being the highest weight given to the current wind speed $u(t)$ and decreasing to $w_{ur} = 1$ when $r = N$.

The maximum of the weighted differences is taken as the gust measure δU_0[5]:

$$\delta U_0 = \max_r \{\Delta U_{window}\}. \tag{9}$$

5.2 | Modified gust measure

It has been observed that the severity of peaks in generator speed is greater if the control is transitioning from R2 to R3. This is due to switching the control actuation from torque control to blade pitch control, with the generator speed near its rated RPM. However, the gust measure as presented above only takes into account the nature of the wind input. In order to improve the correlation between the gust measure and the generator speed peak, we can also account for the proximity of the control to the transition. This can be achieved by applying a similar algorithm to the generator torque signal that accounts for any rise in generator torque toward its saturation limit at rated torque, where the control switches to pitch control in R3. Using a window of generator torque samples similar to that for the wind signal in Equation (5), we have

$$\tau_{window} = \{\tau(t - t_r)\}_{r=0,\ldots,N}. \tag{10}$$

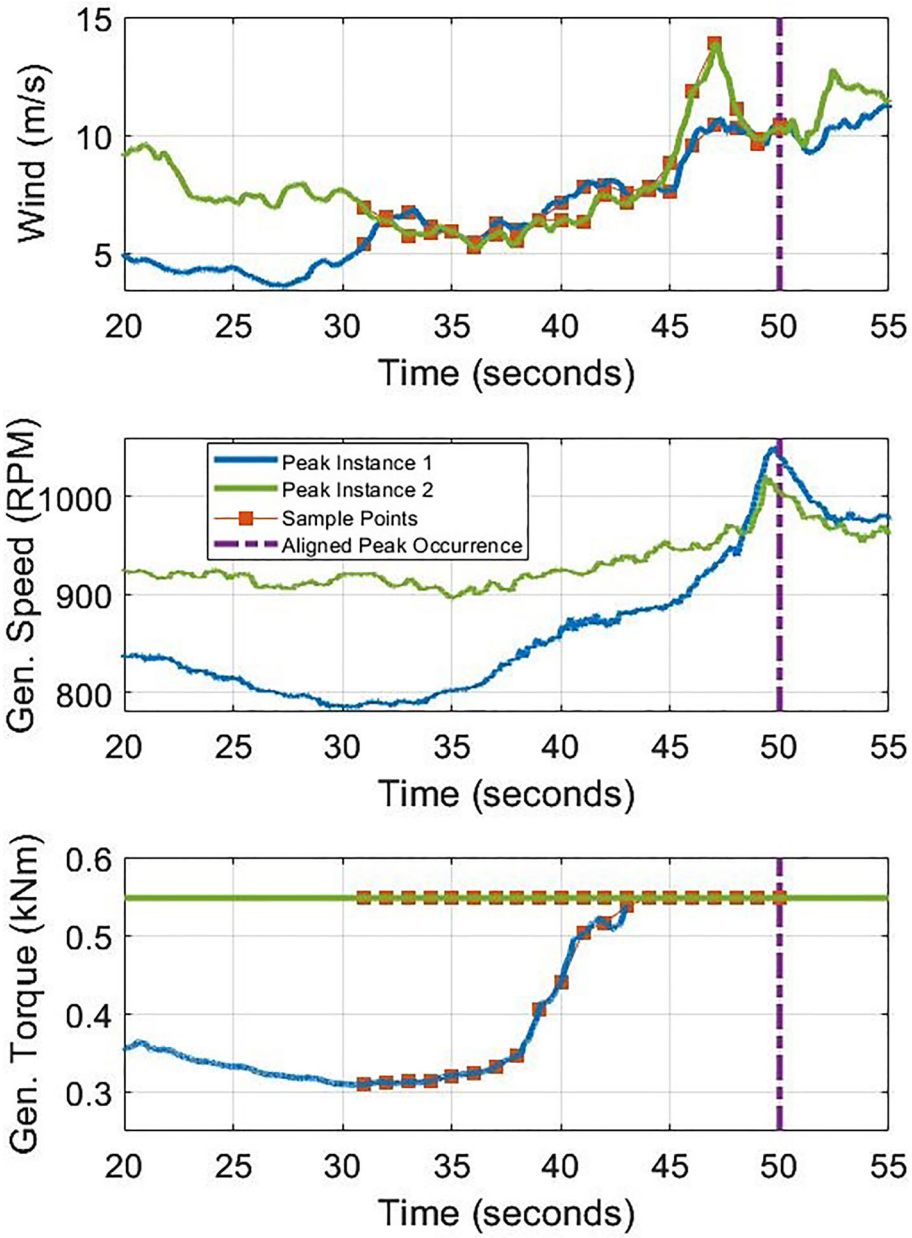

FIGURE 8 Sampling of wind speed and generator torque for modified gust measure δG_0. For Peak Instance 1, the modified gust measure δG_0 is greater than the gust measure δU_0 due to the proximity to a control transition, whereas for Peak Instance 2, both measures are the same since the period leading up to the peak occurs purely in Region 3.

Examples of wind speed and generator torque sampling are shown in Figure 8. Using similar weighted differences as seen in Equations (6)–(9), we obtain a "torque measure" $\delta\tau_0$:

$$\delta\tau_0 = \max_r \{\Delta\tau_{window}\}. \tag{11}$$

The gust measure as shown in Equation (9) can then be modified as the weighted sum of the gust measure and the torque measure:

$$\delta G_0 = k_U \delta U_0 + k_\tau \delta\tau_0, \tag{12}$$

where k_U and k_τ are weighting parameters.

These measures are listed in Table 6, and the tuning parameters for the modified gust measure used for SUMR-D are summarized in Table 7.

5.3 | BL control improvements

The (modified) gust measure(s) are implemented online with the BL controller to mitigate generator overspeed peak occurrences. The gust measure(s) are first tuned to detect possible wind gusts under turbulent wind conditions. A turbine de-rating schedule is then derived to de-rate the turbine for those gust measure values above which a generator overspeed peak is likely. Figure 9 shows the de-rating schedule used for the following SUMR-D simulations. As can be seen, the turbine is at most de-rated to 95% of its nominal rating in the presence of gusts. The de-rating is achieved by reducing the wind speed based reference generator speed set point of the blade pitch control by the factor of the rating as shown in Figure 10.

The results of implementation of the advanced controller using the (modified) gust measure(s) are shown in Figure 11. We compare the performance of the BL control, BL with gust measure (BL + GM), and BL with modified gust measure (BL + MGM) for a field-replicated wind simulation. The two peaks in the generator speed occur near the 280 s mark, where the control switches from R2 to R3 and near the 315 s mark, where the control is only in R3. For the R3 peak, both BL + GM and BL + MGM perform equally better than BL in mitigating the generator speed peak, in contrast to the speed peak in the near-rated region where BL + MGM performs better than BL + GM as it accounts for the control switching regions.

Figure 12A shows the mean, maximum, and minimum generator speeds across wind speeds, comparing simulations of SUMR-D using field-replicated wind conditions. In near above-rated winds (5 to 8 m/s), BL + MGM performs slightly better than BL + GM in reducing the generator speed maxima, whereas in higher wind speeds (8 to 12 m/s), both BL + GM and BL + MGM reduce the maximum generator speed occurrences and on average improve the generator speed regulation to its rated RPM value. Considering the safety margin to be the difference between the generator speed shutdown threshold and the maximum generator speed occurrence across simulations, the safety margin is improved by 29% for BL + GM and by 34% for BL + MGM over the BL performance. This improvement in the safety margin reduces the likelihood of a generator

TABLE 6 Summary of measures.

Measures	Equation	Notes
δU_0	Equation (9)	Gust measure developed in Zalkind et al.[5]
$\delta\tau_0$	Equation (11)	Torque measure for proximity to transition
δG_0	Equation (12)	Modified gust measure

TABLE 7 (Modified) gust measure tuning parameters.

Description	Variable	Value
Number of samples	N	20
Sampling period	Δt	1 s
Highest weight for wind samples	w_{u0}	2.5 $(m/s)^{-1}$
Highest weight for generator torque samples	$w_{\tau 0}$	45 $(kNm)^{-1}$
Weight for gust measure	k_U	1
Weight for torque measure	k_τ	0.55

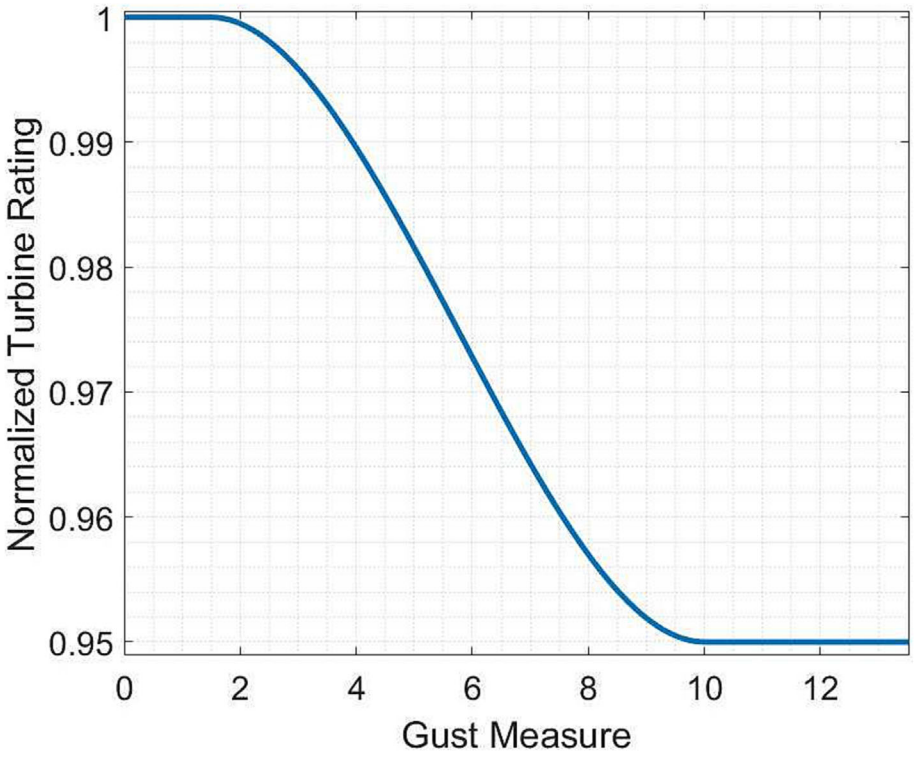

FIGURE 9 Wind turbine de-rating schedule.

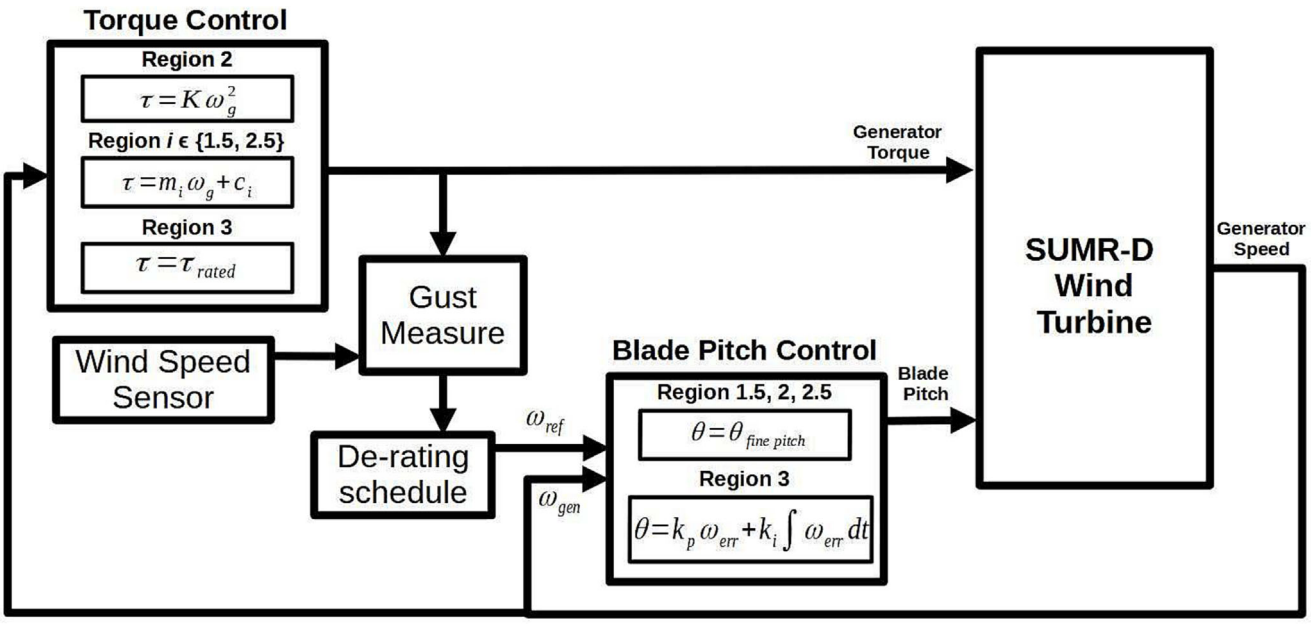

FIGURE 10 SUMR-D advanced control using gust measure.

overspeed event causing the turbine to go out of operation. The improved margin also opens the opportunity to boost the rating of the turbine in periods of lower likelihoods of wind gusts in order to improve the turbine power production. A control feature implementing the boosting of power production based on gust measures is left for future work. A high-turbulence operational DLC 1.3 is also tested with the BL and advanced controllers. The maximum generator speed peak occurrences are shown in Figure 12B. In this case, we can see that the BL control has maximum generator speed occurrences that come very close to the shutdown threshold. The advanced controllers reduce the generator speed maximum occurrences by around 30%.

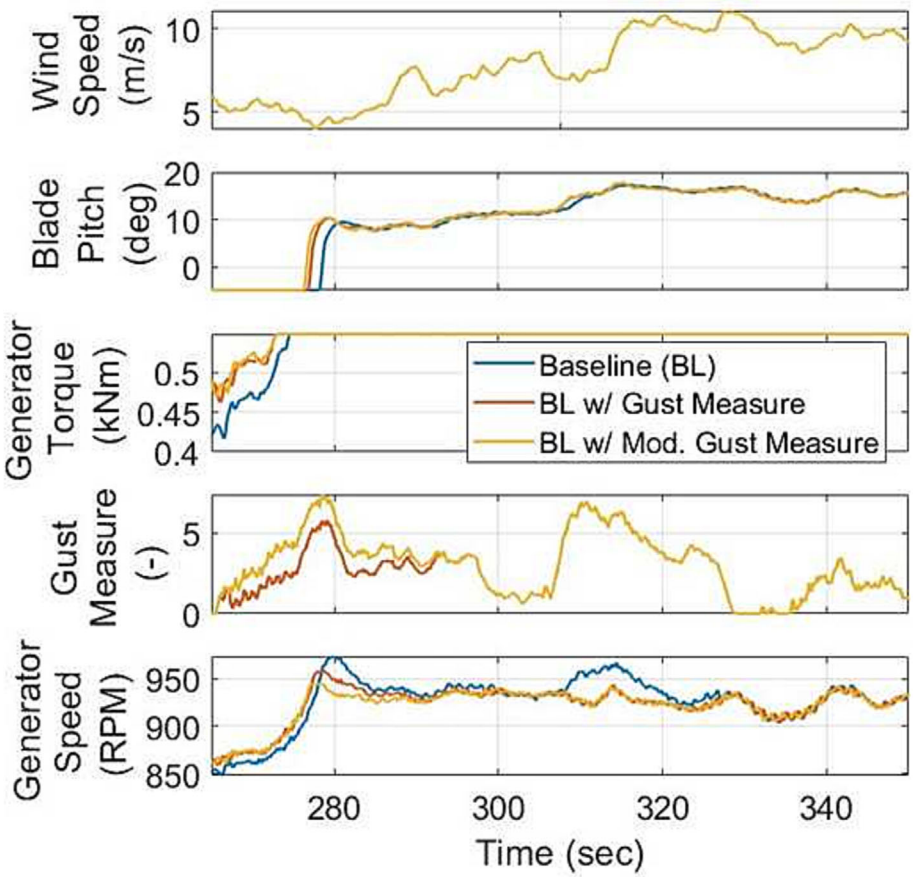

FIGURE 11 Baseline control versus advanced control time series. The same wind field applies in all cases (all curves are coincident in uppermost plot). Since the baseline controller does not use any gust measure, there is no curve for baseline (BL) in the fourth plot.

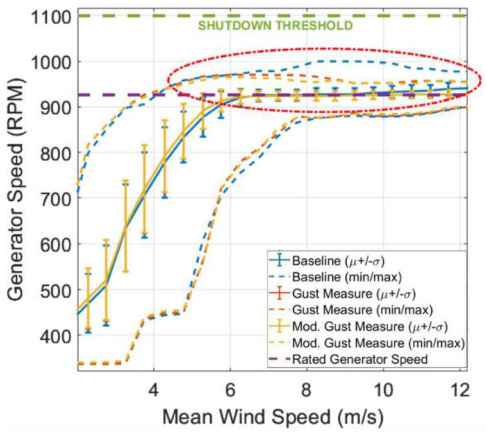

(A) Generator speeds for a subset of field replicated operational wind simulations. The means and standard deviations for the gust measure and the modified gust measure based controls are nearly coincident.

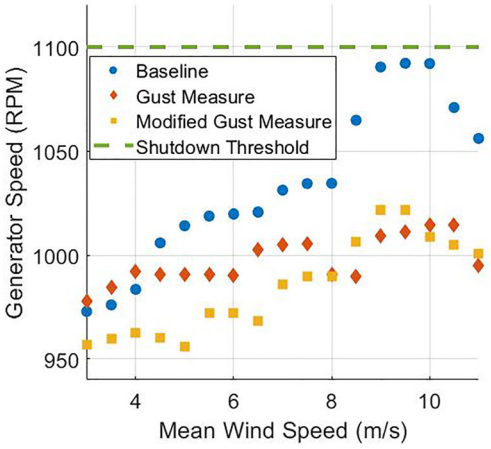

(B) Maximum generator speed occurrences across wind speeds for DLC 1.3

FIGURE 12 Baseline control versus advanced control based on gust measures across wind speeds.

6 | CONCLUSIONS AND RECOMMENDATIONS

This study presents the development of gust-measure-based advanced control techniques to improve generator speed regulation and mitigate overspeed events in high turbulence, gusty wind conditions. The gust measure uses recent wind speeds to predict the likelihood of a particular wind gust event and de-rates the turbine to reduce generator overspeeding. The modified gust measure developed in this research also accounts for the proximity of the turbine operation to the transition from below-rated to above-rated control to further mitigate the generator overspeed peaks. The advanced controllers are tested using realistic wind conditions from the field experiment data of the SUMR-D experimental research rotor tested on the CART2 research turbine platform at NREL's NWTC facility. The SUMR-D aims to replicate the full-scale 13.2 MW SUMR-13 turbine design that explores a two-bladed, downwind rotor configuration to achieve lighter, ultra-flexible blade designs to reduce rotor mass and cost. First an analysis of the field test data of SUMR-D is conducted, to verify the accuracy of the OpenFAST simulation model in representing the actual turbine. We study the wind resource at NWTC for operational SUMR-D data and compare the power and flapwise blade loads under simulated operational DLC 1.2 to conclude that the turbine operated within the expected performance from the simulation model with underestimation of power produced at lower wind speeds. To further validate the turbine model and OpenFAST simulation tool, we replicate turbulent site wind conditions in OpenFAST to conclude that simulated actuator responses and generator outputs are reasonably in agreement with measured values from the field test.

Particular wind gust patterns in the field data are observed to cause peaks in the generator speed response. To mitigate the occurrence of such peaks, the BL controller from the field test is improved using gust estimation techniques to predict the likelihood of an incoming wind gust and to de-rate the turbine as needed to better regulate the generator speed in near- and above-rated wind conditions. The BL and advanced control techniques based on the gust measures are compared using field wind conditions in simulation to confirm that the generator speed response improves with regards to mean and maximum RPMs across wind speeds. The gust-measure-based control is expected to be especially beneficial under high-turbulence intensity wind conditions.

Recommended future work includes development of a wind speed estimator in order to provide a more realistic implementation for determining the gust measures that are used in the advanced control methods presented in this paper. The modified gust measure also provides an opportunity to improve turbine power capture. This can be achieved by dynamically boosting the rating of the turbine when the likelihood of a wind gust is estimated to be low. This has the potential to increase the turbine AEP.[5]

ACKNOWLEDGEMENTS

This work was supported in part by the Advanced Research Projects Agency—Energy (ARPA-e) ATLANTIS Program, under Award Number DE-AR0000667. Any opinions, findings, and conclusions or recommendations expressed in this material are those of the authors and do not necessarily reflect the views of ARPA-e. We would also like to thank Lee Jay Fingersh, Andrew Scholbrock, and the team at NREL for conducting the SUMR-D field tests, gathering and organizing the data, and making it available for analysis. The authors acknowledge the ARPA-E Segmented Ultralight Morphing Rotor (SUMR) team for comments and suggestions throughout the research study. We also gratefully acknowledge support from a Palmer Endowed Chair Professorship at the University of Colorado Boulder and the Hanse-Wissenschaftskolleg in Delmenhorst, Germany. This work was authored in part by the National Renewable Energy Laboratory, operated by Alliance for Sustainable Energy, LLC, for the U.S. Department of Energy (DOE) under Contract No. DE-AC36-08GO28308. The views expressed in the article do not necessarily represent the views of the DOE or the US government. The US government retains and the publisher, by accepting the article for publication, acknowledges that the US government retains a nonexclusive, paid-up, irrevocable, worldwide license to publish or reproduce the published form of this work, or allow others to do so, for US government purposes.

DATA AVAILABILITY STATEMENT

The data that support the findings of this study are stored by NREL and openly available from the Department of Energy Atmosphere to Electrons program via https://a2e.energy.gov/data/sumr-d/turbine.z01.b0.

ORCID

Mandar Phadnis https://orcid.org/0000-0001-5062-4741
Daniel Zalkind https://orcid.org/0000-0003-0482-3285

REFERENCES

1. Veers P, Bottasso C, Manuel L, et al. Grand challenges in the design, manufacture, and operation of future wind turbine systems. *Wind Energ Sci*. 2023;8(7):1071-1131.
2. Pao L, Johnson K. Control of wind turbines. *IEEE Control Syst Mag*. 2011;31(2):44-62.
3. Loth E, Steele A, Qin C, Ichter B, Selig M, Moriarty P. Downwind pre-aligned rotors for extreme-scale wind turbines. *Wind Energy*. 2017;20:1241-1259.

4. Zalkind DS, Pao LY. Constrained wind turbine power control. In: Proceedings of the American Control Conference. IEEE; 2019:3494-3499.
5. Zalkind DS, Nicotra MM, Pao LY. Constrained power reference control for wind turbines. *Wind Energy*. 2022;25(5):914-934.
6. Phadnis M, Pao L. On the severity of wind turbine generator speed peaks in response to particular gusts. In: Proceedings of the American Control Conference. IEEE; 2022:3538-3543.
7. Zalkind D, Pao L, Martin D, Johnson K. Models used for the simulation and control of a segmented ultralight morphing rotor. *IFAC-PapersOnLine*. 2017;50(1):4478-4483.
8. U.S. Department of Energy. Ultra-large wind turbine. https://arpa-e.energy.gov/technologies/projects/ultra-large-wind-turbine
9. U.S. Department of Energy. Segmented Ultralight Morphing Rotor, Demonstrator (SUMR-D). https://a2e.energy.gov/projects/sumr-d
10. Kianbakht S, Martin D, Johnson K, et al. Design space exploration and decision-making for a segmented ultralight morphing 50-MW wind turbine. *Wind Energy*. 2022;25(12):2016-2035.
11. Escalera Mendoza AS, Yao S, Chetan M, Griffith DT. Design and analysis of a segmented blade for a 50 MW wind turbine rotor. *Wind Engineering*. 2022;46(4):1146-1172.
12. Pao L, Zalkind D, Griffith T, et al. Control co-design of 13 MW downwind two-bladed rotors to achieve 25% reduction in levelized cost of wind energy. *Annu Rev Control*. 2021;51:331-343.
13. Yao S, Griffith T, Chetan M, Bay C, Damiani R, Kaminski M, Loth E. A gravo-aeroelastically scaled wind turbine rotor at field prototype scale with strict structural requirements. *Renew Energy*. 2020;156:535-547.
14. Kaminski M, Loth E, Zalkind D, Pao L, Selig M, Johnson K. Servo-aero-gravo-elastic (SAGE) scaling of a 13-MW downwind turbine. *J Renew Sustain Energy*. 2020;12(6):63301.
15. Bay C, Damiani R, Fingersh LJ, et al. Design and testing of a scaled demonstrator turbine at the National Wind Technology Center. In: Proceedings of the AIAA Science and Technology Forum and Exposition. American Institute of Aeronautics and Astronautics; 2019.
16. U.S. Department of Energy. SUMR-D wind turbine/reviewed data. Online https://a2e.energy.gov/data/sumr-d/turbine.z01.b0
17. Bossanyi EA. Individual blade pitch control for load reduction. *Wind Energy: An Int J Progress Appl Wind Power Convers Technol*. 2003;6(2):119-128.
18. Bir G. Multi-blade coordinate transformation and its application to wind turbine analysis. In: 46th AIAA Aerospace Sciences Meeting and Exhibit. American Institute of Aeronautics and Astronautics; 2008:1300.
19. Namik H, Stol K. Disturbance accommodating control of floating offshore wind turbines. In: 47th AIAA Aerospace Sciences Meeting Including the New Horizons Forum and Aerospace Exposition. American Institute of Aeronautics and Astronautics; 2009:483.
20. Kim K, Kim H-G, Paek I. Application and validation of peak shaving to improve performance of a 100 kW wind turbine. *Int J Precis Eng Manuf-Green Technol*. 2020;7:411-421.
21. Feil R, Abbas N, Bortolotti P, Johnson N, Mertz B. Distributed aerodynamic control using active trailing-edge flaps for large wind turbines. *J Phys: Conf Ser*. 2020;1618(4):42026.
22. Bernhammer LO. Smart Wind Turbine: Analysis and Autonomous Flap. *Doctoral thesis*. TU Delft; 2015.
23. Abbas NJ, Bortolotti P, Kelley C, Paquette J, Pao L, Johnson N. Aero-servo-elastic co-optimization of large wind turbine blades with distributed aerodynamic control devices. *Wind Energy*. 2023;26(8):763-785.
24. Bossanyi E, Wright A, Fleming P. Controller Field Tests on the NREL CART2 Turbine. NREL/TP-5000-49085, National Renewable Energy Laboratory; 2010.
25. Selig M. PROPID—software for horizontal-axis wind turbine design and analysis. 1995. Online http://www.ae.illinois.edu/m-selig/propid.html
26. Selig M, Maughmert M. Generalized multipoint inverse airfoil design. *AIAA J*. 1992;30(11):2618-2625.
27. Ananda G, Bansal S, Selig M. Aerodynamic design of the 13.2 MW SUMR-13i wind turbine rotor. In: 2018 Wind Energy Symposium. American Institute of Aeronautics and Astronautics; 2018:1-18.
28. ANSYS Inc. 2018. Online https://www.ansys.com
29. NREL. OpenFAST. Accessed November 12, 2019. https://github.com/OpenFAST/openfast
30. Albers A. *Turbulence and Shear Normalisation of Wind Turbine Power Curve*. Deutsche WindGuard Consulting GmbH; 2010.
31. IEC:61400-12-1. Wind Turbines—Part 12-1: Power Performance Measurements of Electricity Producing Wind turbines, International Electrotechnical Commission; 2016. Tech. rep.
32. Pereira D. Wind Rose. MATLAB Central File Exchange; 2022. https://www.mathworks.com/matlabcentral/fileexchange/47248-wind-rose
33. IEC:61400-1. Wind Turbines—Part 1: Design Requirements, International Electrotechnical Commission; 2005. Tech. rep.
34. MathWorks. Simulink: simulation and model-based design; 2020.
35. Jonkman BJ. *TurbSim User's Guide v2.00.00*: National Renewable Energy Laboratory; 2014.

How to cite this article: Phadnis M, Zalkind D, Pao L. Advanced wind turbine control development using field test analysis for generator overspeed mitigation. *Wind Energy*. 2024;27(11):1188-1204. doi:10.1002/we.2860